Wind tunnel measurements of sphere drag at supersonic speeds and low Reynolds numbers

By PETER P. WEGENER† AND HARRY ASHKENAS

Jet Propulsion Laboratory, California Institute of Technology, Pasadena, California

(Received 23 January 1961)

Sphere drag has been measured in a low-density supersonic wind tunnel by a simple displacement technique. A conical nozzle of fixed geometry, operated at a constant supply temperature of about 300 °K was used. Test section Mach numbers ranged between 3·8 and 4·3 depending on supply pressure. The Reynolds number and Knudsen number range, based on free-stream conditions and sphere diameter, were $50 < Re_\infty < 1000$ and $0{\cdot}106 < Kn_\infty < 0{\cdot}006$, respectively. This range was achieved by varying sphere size and supply pressure. The drag coefficient was found to increase from a value of $C_D = 1{\cdot}17$ at $Re_\infty = 1000$ to $C_D = 1{\cdot}73$ at $Re_\infty = 50$.

1. Introduction

The determination of sphere drag has long been a classical problem in aerodynamics. Unfortunately, few reliable experimental results are available at supersonic speeds and at Reynolds numbers below about 2000. We find in the literature the pioneering low density supersonic wind tunnel experiments by Kane (1951), Sherman (1951), and Jensen (1951) of the University of California at Berkeley covering a Reynolds number range from $Re_\infty = 10$ to that characteristic of the continuum regime for $2 < M < 2{\cdot}8$. In the early days of low-density experiments, however, incomplete knowledge of the flow structure in the test section with resulting uncertainties about the sphere wake (and hence the base drag) cast some doubt on the results reported in Kane (1951), Sherman (1951), and Jensen (1951).‡ Other results have been obtained in firing ranges by May (1957) and May & Witt (1953), of the U.S. Naval Ordnance Laboratory down to $Re_\infty = 1140$ and $Re_\infty = 485$, respectively, for $0{\cdot}82 < M < 4{\cdot}69$. The scatter of firing range data obtained at low Reynolds numbers is relatively large because of the small decrease of flight speed in the range at the low densities. The sphere surface temperature of the Berkeley wind tunnel experiments may be taken to be constant and equal to a mean recovery temperature close to the supply temperature. The range data surface temperatures are undetermined, and, depending on the sphere material, the time of flight, and the ambient density, they range from room temperature to flight temperatures.

There are no complete calculations of sphere drag in the transitional flight régime between continuum and free-molecule flows. Free-molecule results are

† Now at Yale University, New Haven, Connecticut.

‡ Private communication from Prof. F. Sherman, University of California, Berkeley, California.

available from the analytical work of Heineman (1948), who considered the limiting cases of diffuse and specular reflexion in supersonic flow, arriving at values of the drag coefficient, much above the continuum value ($C_D \simeq 1$) for supersonic speeds.

In order to resolve this unsatisfactory state of affairs and to gain a basis for comparison with future theoretical work, it was decided to measure again sphere drag in the transitional flow régime. In particular, a simple method not involving a balance system appeared appropriate to determine the very low values of the drag. This technique consisted of measuring the deflexion of a sphere of known weight and diameter in the supersonic air stream of a low-density tunnel.

2. Experimental methods

The experiments were conducted in the low-density gas dynamics facility, illustrated in figure 1, at the Jet Propulsion Laboratory. Continuous flow in a Mach number range of 3·8–4·3 for free-stream static pressures of 30–100 μ can

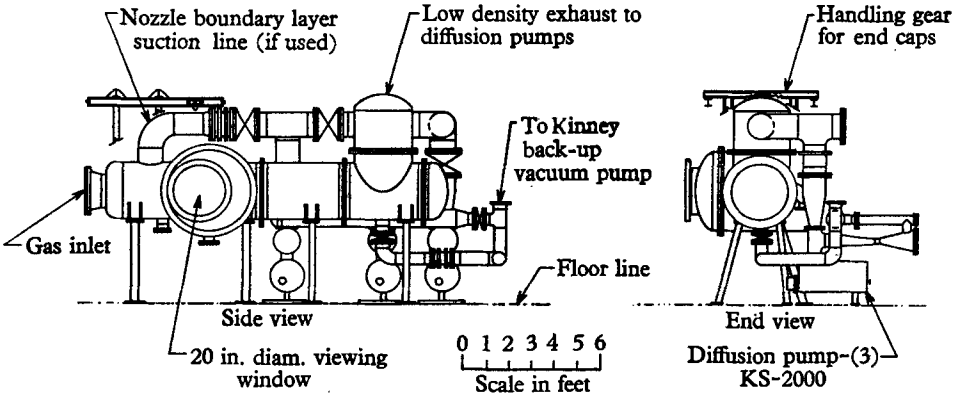

FIGURE 1. Jet propulsion laboratory low-density gas dynamics facility.

be achieved for dry air initially at room temperature. The nozzle exit and the traversing mechanism with a Pitot pressure probe installed are shown in figure 2, plate 1. This system allows traversing in three mutually perpendicular directions; 10 in. of travel are available in the horizontal and vertical cross-flow directions for a fixed position of the base of the system. The device is equipped with reversing motors and two-speed magnetically engaged transmissions; counters on the precision lead screws may be used to determine position to the nearest 0·001 in., or, alternatively, an analog position signal is provided by linear potentiometers.

A simple conical supersonic nozzle with an exit diameter of 2·28 in. was used for the experiments. The usable width of the isentropic core of the flow and, correspondingly, the flow Mach number depend on the supply pressure as seen in the pitot pressure profiles taken at right angles to the flow and 0·5 in. downstream from the nozzle exit (figure 3). The pitot pressure p_0' was measured with a U-tube silicone-oil manometer in the tunnel (figure 2); the fluid level height was determined with an external cathetometer. The pitot tube diameter was chosen to

be large enough to ensure the absence of viscous effects according to the criteria established by Sherman (1955). The supply pressure p_0 was determined with a Betz manometer filled with silicone oil, and the flow Mach number of the isentropic core was found from the ratio p_0'/p_0, using an isentropic flow table. All other required flow parameters were also found from the flow table and the measured supply conditions. Since the conical nozzle does not produce uniform flow in the test section, the Mach number increases with distance in the x-direction. In figure 4, the variation of centreline Mach number with supply pressure is seen clearly. The calibration data of figures 3 and 4 are used to determine all flow conditions shown subsequently, and a given free-stream value was assigned to the stagnation point of the sphere.

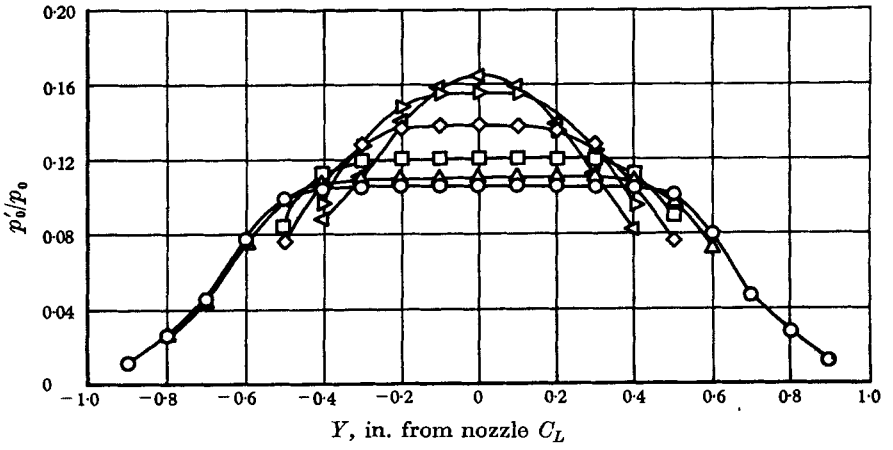

FIGURE 3. Pitot pressure profiles; horizontal traverse across jet; ½ in. downstream from nozzle exit. $T_0 = 300$ °K.

	p_0 mm Hg	p_∞ μ Hg	$M_\infty(p_0'/p_0)$
○	15·81	93	4·322
△	13·76	85	4·279
□	10·34	73	4·171
◇	6·89	61	4·008
▷	5·16	51	3·869
◁	3·46	48	3·784

The method of drag determination is shown schematically in figure 5. A steel or bronze ball-bearing is suspended from the traversing mechanism on a fine (0·00015 to 0·001 in. diameter) tungsten wire; the sphere stagnation point is located ½ in. downstream from the nozzle exit on the nozzle centreline. The air is then turned on and the sphere is blown downstream until an equilibrium position, determined by the drag and weight, is reached. The traversing mechanism is used next to return the sphere to its original, undeflected position, and the distance travelled is found on the traverse counter as Δx in figure 5.

The sphere is stabilized in the airstream by suspending a second damping sphere immersed in an oil bath outside the airstream below the model. In order to specify the geometry completely, the length of the suspension wire, L, is measured

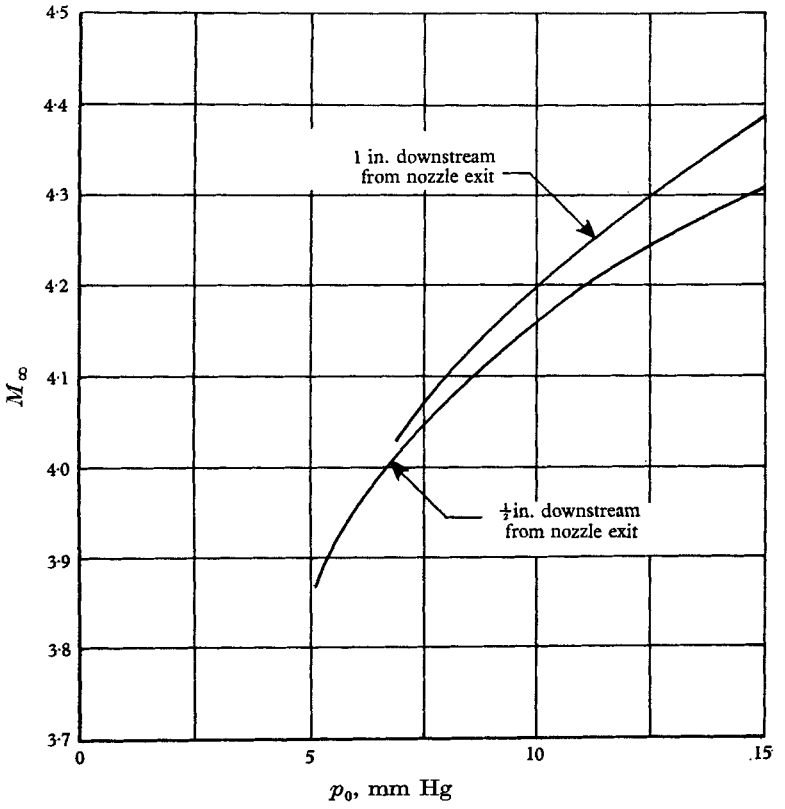

FIGURE 4. Free-stream Mach number dependence on stagnation pressure. 295 °K $\leqslant T_0 \leqslant$ 300 °K.

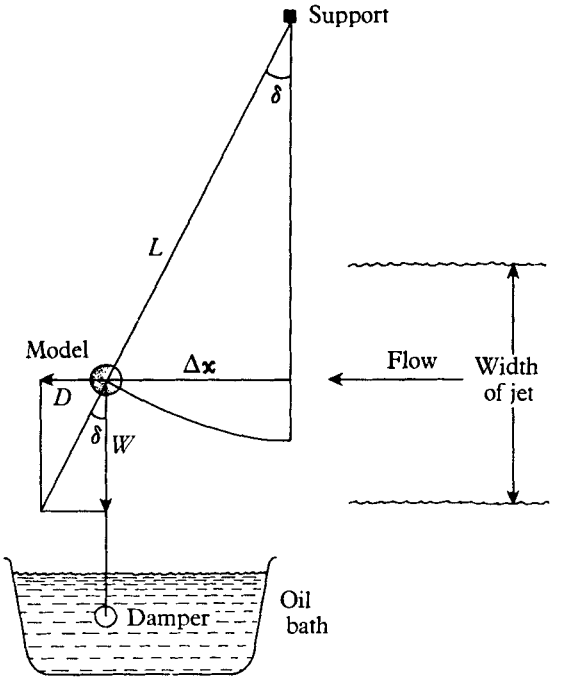

FIGURE 5. Geometry of sphere-drag measurement.

with a cathetometer. The total drag of the sphere and suspension wire D_T is determined from the measured geometry and the measured weight of model plus damper, W.

Thus, we have

$$D_T = (W - b)\tan(\sin^{-1}\Delta x/L), \tag{1}$$

where $D_T = D_{\text{wire}} + D_{\text{sphere}}$ and b = buoyancy force on damper-sphere $= V_d \rho_{\text{oil}}\, g$ = (damper-sphere volume) (density of oil) (acceleration of gravity).

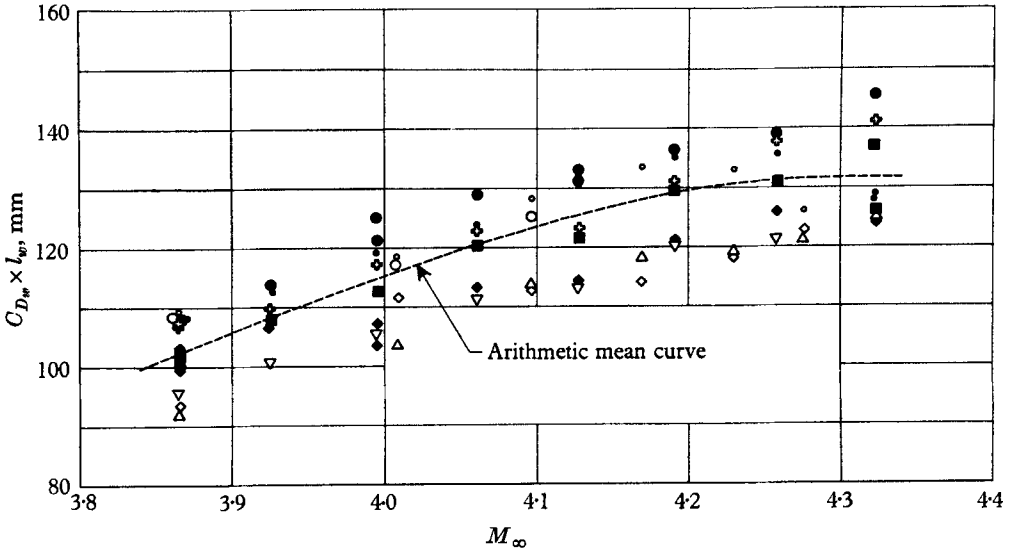

FIGURE 7. Support-wire drag coefficient. Wire diameter, in.: ◇, ◆, 0·001; ○, ●, 0·00068; △, ▽, 0·0005; ○, ●, 0·0003; ✣, 0·00015; □, ■, 0·0002.

In order to separate the wire drag from that of the sphere, measurements of the wire drag alone were made, as illustrated in figure 6, plate 2. The wire was suspended from the traversing mechanism, and a nylon sphere was used to damp the motion of the wire. As the photograph shows, the wire is blown by the airstream to some equilibrium position; the balance of forces on the wire is determined by the angle assumed by the upper straight portion of the wire and the measured weight of wire and damper. An optical comparator is used to determine the angular position from a photographic negative by reference to the plumb bob shown. The wire-drag data were reduced to the wire-drag coefficient shown as a function of Mach number in figure 7. The wire-drag coefficient is defined by

$$C_{D_w} = D_w/(q_\infty l_w d_w), \tag{2}$$

where l_w = wire length, d_w = wire diameter, D_w = wire drag, and q_∞ = free-stream dynamic pressure. The scatter in these data is of the order of $\pm$ 10 %, thus in order to minimize the effect of wire-drag uncertainty on the sphere-drag results, the wire size was reduced as sphere size decreased; in any case, for the results reported here, the wire drag never exceeded 15 % of the total drag D_T. The Knudsen number of the wires, based on free-stream conditions, ranged from 6 to

43; therefore, in principle, wire drag may be computed from free-molecule theory, e.g. for adiabatic surface conditions and diffuse reflexion. Such a comparison was, however, unsuccessful at the lower Mach numbers with the correspondingly large boundary-layer thicknesses through which the wire extended; therefore the current corrections are purely empirical.

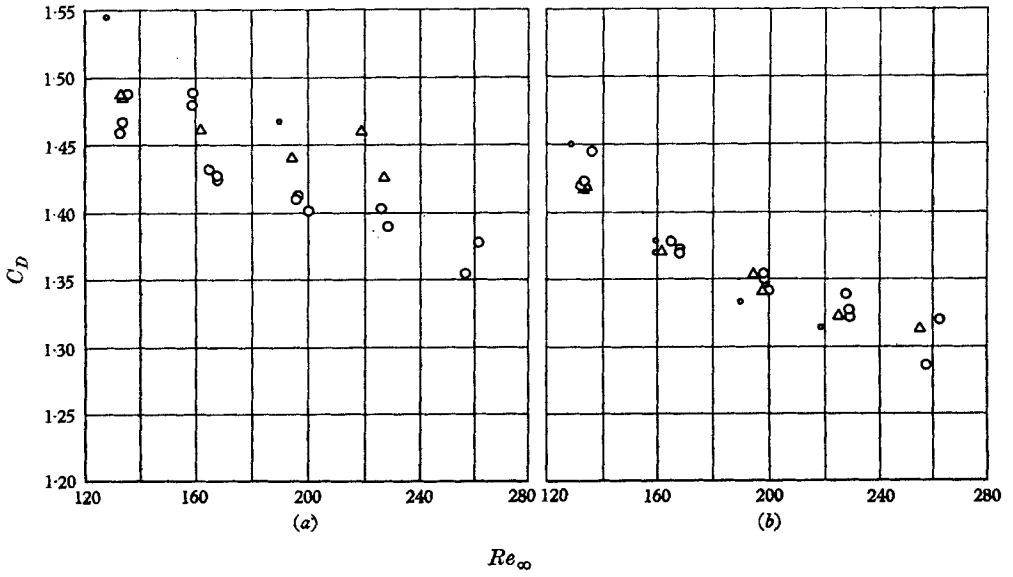

FIGURE 8. Effect of wire-drag correction on drag of $\frac{5}{32}$ in. diameter sphere. Wire diameter, in.: o, 0·00068; △, 0·0005; ○, 0·0003. (*a*) Uncorrected for wire drag. (*b*) Corrected for wire drag; wire drag obtained by direct measurement.

The drag coefficient of the sphere is defined by

$$C_D = \frac{D_s}{q_\infty A_s}, \tag{3}$$

where A_s is the cross-sectional area of the sphere. Combining (1) and (3) and including the correction for the drag of the supporting wire, the drag coefficient becomes

$$C_D = \frac{4}{\pi d_s^2}\left[\frac{(W-b)\tan(\sin^{-1}\Delta x/L)}{q} - C_{D_w} l_w d_w \left(\frac{l_w - d_s}{l_w}\right)\right], \tag{4}$$

where d_s is the diameter of the sphere, and the correction for finite support drag is modified by the masking effect of the sphere on the wire; l_w is taken arbitrarily as the jet width where the dimensionless pitot-pressure plotted in figure 3 had dropped to 90 % of its centreline value.

The magnitude of the wire-drag correction in a restricted Reynolds number range is shown in figure 8, where a comparison is made between corrected and uncorrected drag data.

3. Results and discussion

Excerpts of the results for the series of experiments reported here are shown in table 1. In addition to the final corrected drag coefficient C_D, the free-stream Mach number M_∞, the supply temperature T_0, the free-stream Reynolds number Re_∞, the free-stream Knudsen number Kn_∞, the Reynolds number based on conditions behind the shock wave Re_s, and the Knudsen number behind the shock wave Kn_s are presented. For the calculation of Re_s, the viscosity was based on

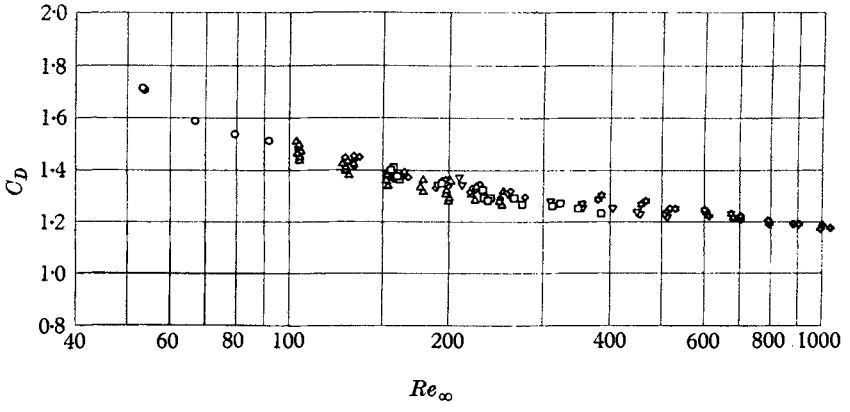

FIGURE 9. Sphere drag; $3{\cdot}8 \leqslant M_\infty \leqslant 4{\cdot}3$; $0{\cdot}013 \leqslant Kn \leqslant 0{\cdot}200$. Sphere diameter in.: ○, $\frac{1}{16}$; △, $\frac{1}{8}$; ◇, $\frac{5}{32}$; □, $\frac{3}{16}$; ▽, $\frac{1}{4}$; ✲, $\frac{3}{8}$; ✣, $\frac{1}{2}$.

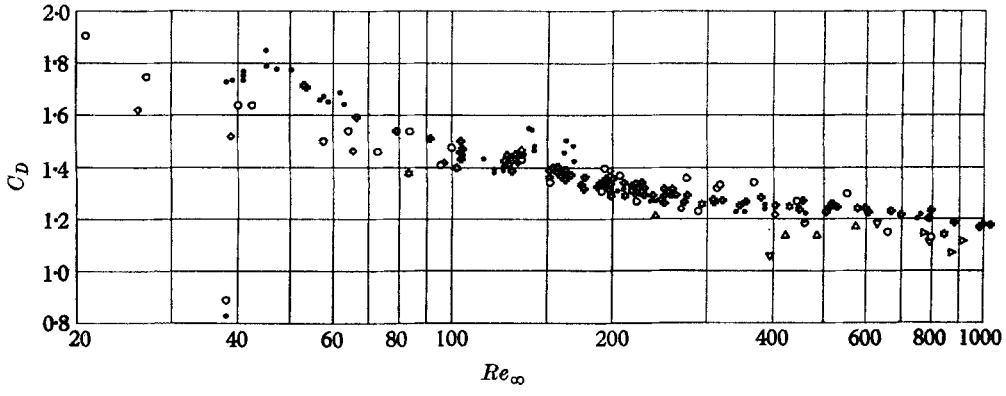

FIGURE 10. Sphere drag; present data compared with earlier investigations.

	M_∞	
○	$2{\cdot}0 < M < 2{\cdot}99$	Wind tunnel data
∘	$2{\cdot}0 < M < 2{\cdot}99$	
◇	$2{\cdot}0 < M < 2{\cdot}99$	
✲	$3{\cdot}0 < M < 3{\cdot}99$	
△	$1{\cdot}0 < M < 1{\cdot}99$	Range data
▽	$2{\cdot}0 < M < 2{\cdot}99$	
▷	$3{\cdot}0 < M < 3{\cdot}99$	
✣	$3{\cdot}8 < M < 4{\cdot}30$	This report: wind tunnel data.

Sphere diameter d_s, in.	T_0, °C	M_∞	Re_∞	Re_s	Kn_∞	Kn_s	C_D
$\frac{1}{16}$	20·1	3·865	53·4	15·5	0·1071	0·0419	1·713
	19·1	3·865	53·6	15·5	0·0167	0·0419	1·709
	19·3	4·007	66·3	18·2	0·0894	0·0354	1·593
	19·6	4·097	79·0	21·0	0·0767	0·0305	1·543
	19·8	4·170	91·3	23·6	0·0675	0·0270	1·508
$\frac{1}{8}$	24·9	3·865	104	30·3	0·0550	0·0214	1·506
	24·9	3·865	104	30·3	0·0550	0·0214	1·498
	24·3	3·862	104	30·3	0·0550	0·0214	1·463
	24·0	3·864	104	30·3	0·0550	0·0214	1·450
	24·2	3·867	105	30·6	0·0545	0·0212	1·511
	22·4	3·866	105	30·4	0·0545	0·0214	1·473
	22·5	3·860	105	30·6	0·0544	0·0212	1·438
	24·8	4·007	127	35·0	0·0467	0·0184	1·428
	24·0	4·008	128	35·2	0·0463	0·0183	1·415
	24·3	4·008	128	35·3	0·0463	0·0182	1·402
	22·5	4·008	130	35·8	0·0456	0·0180	1·383
	24·0	4·096	152	40·6	0·0399	0·0158	1·361
	24·0	4·096	152	40·6	0·0399	0·0158	1·350
	24·9	4·096	154	41·1	0·0394	0·0156	1·396
	22·5	4·097	154	41·0	0·0394	0·0156	1·343
	24·1	4·169	176	45·4	0·0350	0·0140	1·337
	22·5	4·170	177	45·7	0·0349	0·0139	1·316
	24·8	4·169	178	46·1	0·0347	0·0138	1·373
	24·1	4·230	199	50·3	0·0314	0·0123	1·324
	24·1	4·299	199	50·3	0·0314	0·0126	1·316
	24·8	4·230	201	50·8	0·0311	0·0125	1·359
	22·5	4·230	201	50·6	0·0311	0·0126	1·300
	22·5	4·230	201	50·6	0·0311	0·0126	1·292
	24·3	4·276	221	54·8	0·0286	0·0116	1·312
	22·5	4·276	223	55·3	0·0284	0·0114	1·288
	24·9	4·276	225	56·0	0·0281	0·0113	1·343
	24·3	4·323	248	60·5	0·0258	0·0104	1·281
	22·7	4·325	250	61·0	0·0256	0·0104	1·267
	24·9	4·323	252	61·5	0·0254	0·0103	1·324
$\frac{5}{32}$	26·8	3·863	128	37·4	0·0447	0·0174	1·452
	26·1	3·864	129	37·7	0·0443	0·0172	1·430
	20·6	3·866	133	38·6	0·0430	0·0168	1·446
	20·8	3·866	133	38·6	0·0430	0·0168	1·425
	20·1	3·866	134	38·9	0·0427	0·0167	1·452
	18·6	3·867	134	38·9	0·0427	0·0167	1·418
	17·4	3·867	136	39·3	0·0421	0·0165	1·447
	26·5	4·007	159	43·9	0·0373	0·0146	1·370
	20·7	4·008	165	45·4	0·0360	0·0142	1·394
	21·0	4·008	165	45·4	0·0360	0·0142	1·380
	17·6	4·010	168	46·0	0·0353	0·0140	1·371
	26·6	4·096	190	50·7	0·0319	0·0126	1·336
	19·1	4·098	195	51·7	0·0311	0·0124	1·355
	21·2	4·097	196	52·1	0·0309	0·0123	1·353
	17·8	4·098	200	53·0	0·0303	0·0121	1·342
	26·7	4·169	220	57·0	0·0280	0·0112	1·328

TABLE 1. Sphere drag data

Sphere diameter d_s, in.	T_0, °C	M_∞	Re_∞	Re_s	Kn_∞	Kn_s	C_D
$\frac{5}{32}$	19·1	4·171	225	57·8	0·0274	0·0110	1·324
	21·3	4·170	226	58·3	0·0273	0·0109	1·340
	20·8	4·170	228	58·8	3·0271	0·0108	1·344
	26·7	4·229	249	63·0	0·0251	0·0101	1·290
	18·1	4·231	262	66·0	0·0239	0·00962	1·321
	26·7	4·275	278	69·2	0·0228	0·00915	1·298
	27·0	4·322	312	76·4	0·0203	0·00827	1·275
$\frac{3}{16}$	24·2	3·866	157	45·7	0·0364	0·0142	1·399
	21·8	3·865	158	46·0	0·0362	0·0141	1·398
	17·8	3·867	162	46·8	0·0353	0·0139	1·360
	24·3	4·007	194	53·5	0·0306	0·0120	1·345
	18·1	4·009	201	55·1	0·0295	0·0117	1·304
	24·4	4·097	232	61·9	0·0261	0·0103	1·391
	24·4	4·097	232	61·9	0·0261	0·0103	1·317
	18·8	4·098	239	63·3	0·0254	0·0101	1·282
	18·3	4·098	240	63·6	0·0253	0·0101	1·289
	24·4	4·169	265	68·4	0·0233	0·0093	1·293
	18·6	4·171	276	70·9	0·0224	0·0089	1·270
	18·6	4·231	313	78·9	0·0200	0·0080	1·264
	18·8	4·231	313	78·9	0·0200	0·0080	1·258
	18·6	4·277	350	86·8	0·0181	0·0073	1·248
	19·0	4·324	392	95·2	0·0163	0·0066	1·229
$\frac{1}{4}$	23·7	3·865	209	60·8	0·0274	0·01067	1·374
	22·3	3·867	212	61·5	0·0270	0·01055	1·342
	23·8	4·009	255	70·1	0·0233	0·00917	1·306
	22·3	4·009	262	72·0	0·0226	0·00893	1·301
	23·8	4·097	310	82·8	0·0196	0·00773	1·277
	23·7	4·169	358	92·4	0·0172	0·00689	1·265
	22·6	4·171	361	93·1	0·0171	0·00684	1·259
	23·7	4·230	406	102	0·0154	0·00623	1·252
	23·5	4·276	453	112	0·0140	0·00566	1·235
	22·6	4·276	456	113	0·0139	0·00561	1·229
	22·7	4·323	506	123	0·0126	0·00514	1·218
$\frac{3}{8}$	25·6	4·007	385	106	0·0154	0·00607	1·287
	25·6	4·096	460	123	0·0132	0·00520	1·269
	24·9	4·096	462	123	0·0131	0·00520	1·267
	25·6	4·169	532	138	0·0116	0·00462	1·254
	24·8	4·170	534	138	0·0116	0·00462	1·249
	25·6	4·229	602	152	0·0104	0·00418	1·244
	24·6	4·230	605	153	0·0103	0·00415	1·241
	25·5	4·275	672	167	0·0094	0·00379	1·227
	24·6	4·275	676	168	0·0094	0·00377	1·227
$\frac{1}{2}$	26·5	4·007	509	140	0·0116	0·00460	1·254
	26·2	4·007	512	141	0·0116	0·00456	1·247
	26·2	4·096	612	163	0·0099	0·00393	1·226
	26·5	4·169	704	182	0·0088	0·00350	1·220
	26·2	4·169	707	183	0·0087	0·00348	1·213
	27·5	4·229	794	202	0·0079	0·00314	1·206
	26·2	4·228	800	202	0·0078	0·00314	1·197
	26·1	4·275	894	223	0·0071	0·00284	1·190
	26·1	4·322	1004	246	0·0064	0·00257	1·177

TABLE 1 (*cont.*)

T_s, the free-stream temperature behind the normal shock wave. Viscosity, where it enters the above parameters, was determined as a function of temperature from Sutherland's law for $T > 110{\cdot}4\,°\mathrm{K}$. For temperatures below 110·4 °K, Van Driest's approximation (1954), in which the viscosity-temperature relation is taken to be the tangent to the Sutherland curve at 110·4 °K, was used. The sphere-drag coefficient is shown in figure 9 as a function of free-stream Reynolds number for spheres of different sizes. In figure 10 these results are compared with those previously cited. It is seen that the scatter of the current experiments is generally satisfactory and that the results for $Re_\infty > 100$ agree with the range of the older experimental findings. At the low Reynolds numbers, the present results appear to give an upper bound of the data.

There clearly exists the need for further data at even lower Reynolds numbers. The data of table 1 have been plotted with the drag coefficient as a function of free-stream Knudsen number and of Reynolds and Knudsen numbers based on conditions behind the shock. These curves are not shown here, as no improvement in the correlation is to be noted. However, the flow state was known well enough to permit the calculation of these variables, and they are included for later use when comparisons with results obtained in high-temperature facilities become available. Such results ought to be correlated on the basis of conditions behind the shock-wave.

Finally, several practical points concerning these experiments must be noted.

1. The pull on the damper sphere wire due to surface tension in the oil at the oil surface may be neglected.

2. The Mach number gradient in the tunnel airstream of 0·1/in. has no noticeable effect on the drag of the smaller diameter spheres, as evidenced by the complete overlap of the drag data for these models as seen in figure 9. The larger models (e.g. those of $\frac{1}{2}$ and $\frac{3}{8}$ in. diameter) exhibit a small but definite deviation in the overlapping ranges. This may be partially due to the Mach number gradient; additionally, the model size approaches the core diameter of the stream, and this also gives rise to error. No jet boundary interference corrections have been applied to the present data.

3. Drag measurements obtained after several hours of continuous tunnel operation showed no sensible deviation from values obtained after only 10 minutes of operation. Therefore it is presumed that all the measurements presented represent the equilibrium wall temperature drag, although no attempts were made to measure the surface temperature of the model.

This paper presents the results of one phase of research carried out at the Jet Propulsion Laboratory, California Institute of Technology, under joint sponsorship of the Department of the Army, Ordnance Corps (under contract no. Da-04-495-Ord 18), and the Department of the Air Force.

The authors wish to acknowledge the work of H. N. Riise, who provided the nozzle calibration data, S. B. Wheeler, whose painstaking construction of the model suspensions is in large measure responsible for the success of the experiments, and A. C. Bouck, whose operation of the tunnel and assistance in the measurements is greatly appreciated.

REFERENCES

HEINEMAN, M. 1948 Theory of drag in highly rarefied gases. *Comm. Appl. Math.* **1**, 259–73.

JENSEN, N. A. 1951 Supplementary data on sphere drag tests. Part 2. *Univ. Calif., Inst. Engng. Res.* HE-150-92.

KANE, E. D. 1951 Sphere drag data at supersonic speeds and low Reynolds numbers. *J. Aero. Sci.* **18**, 259–70.

MAY, A. 1957 Supersonic drag of spheres at low Reynolds numbers in free flight. *J. Appl. Phys.* **28**, 910–12.

MAY, A. & WITT, W. R. 1953 Free flight determinations of the drag coefficients of spheres. *J. Aero. Sci.* **20**, 635–38.

SHERMAN, F. S. 1951 Note on sphere drag data. *J. Aero. Sci.* **18**, 566.

SHERMAN, F. S. 1955 New experiments on impact pressure interpretation in supersonic and subsonic rarefied airstreams. *NACA TN* 2995.

VAN DRIEST, E. R. 1954 The laminar boundary layer with variable fluid properties. *Report AL-1866, North American Aviation Co., Downey, California.*

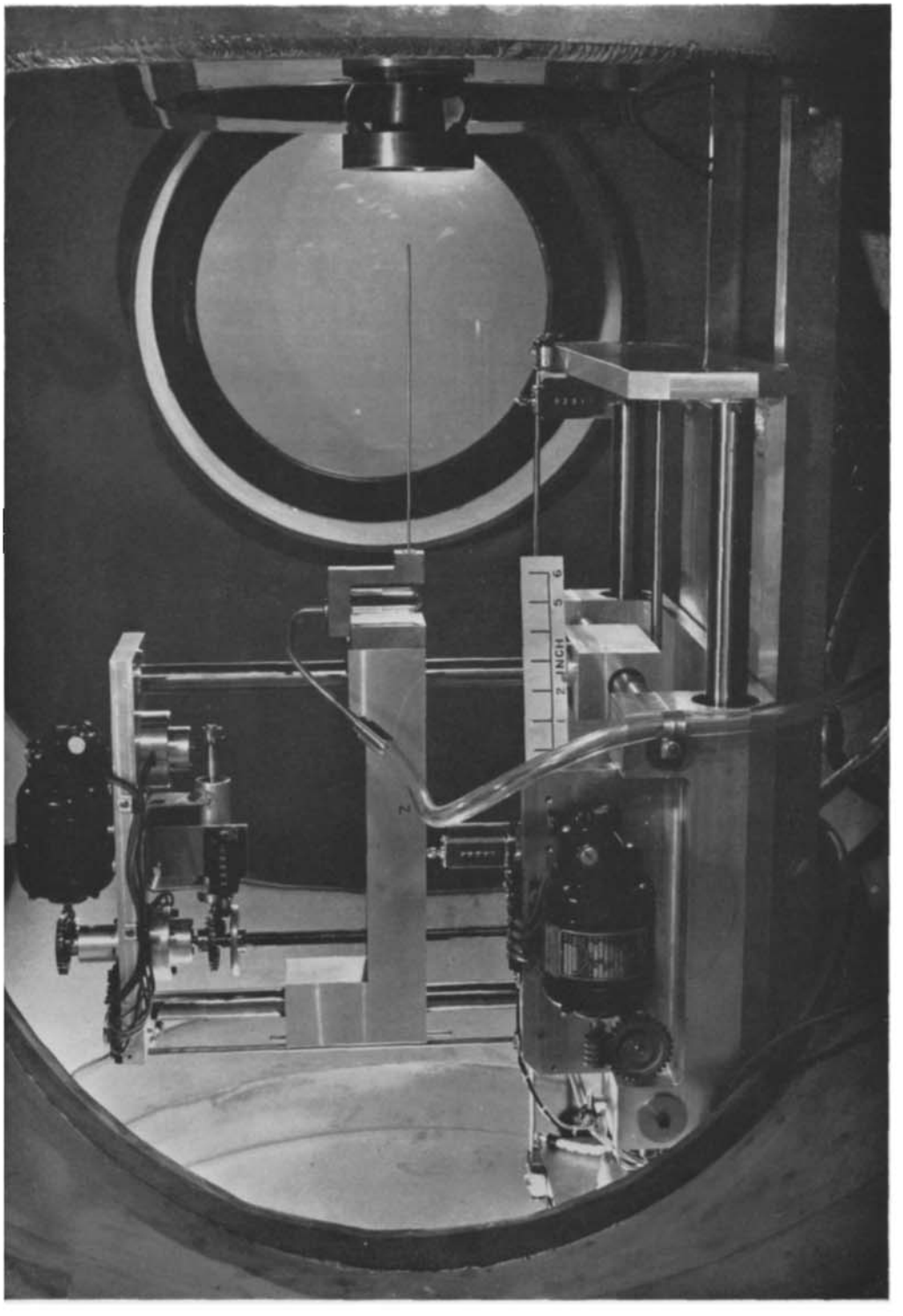

FIGURE 2. Traversing mechanism with instrumentation for tunnel calibration; $M = 4$ (nominal) nozzle at right.

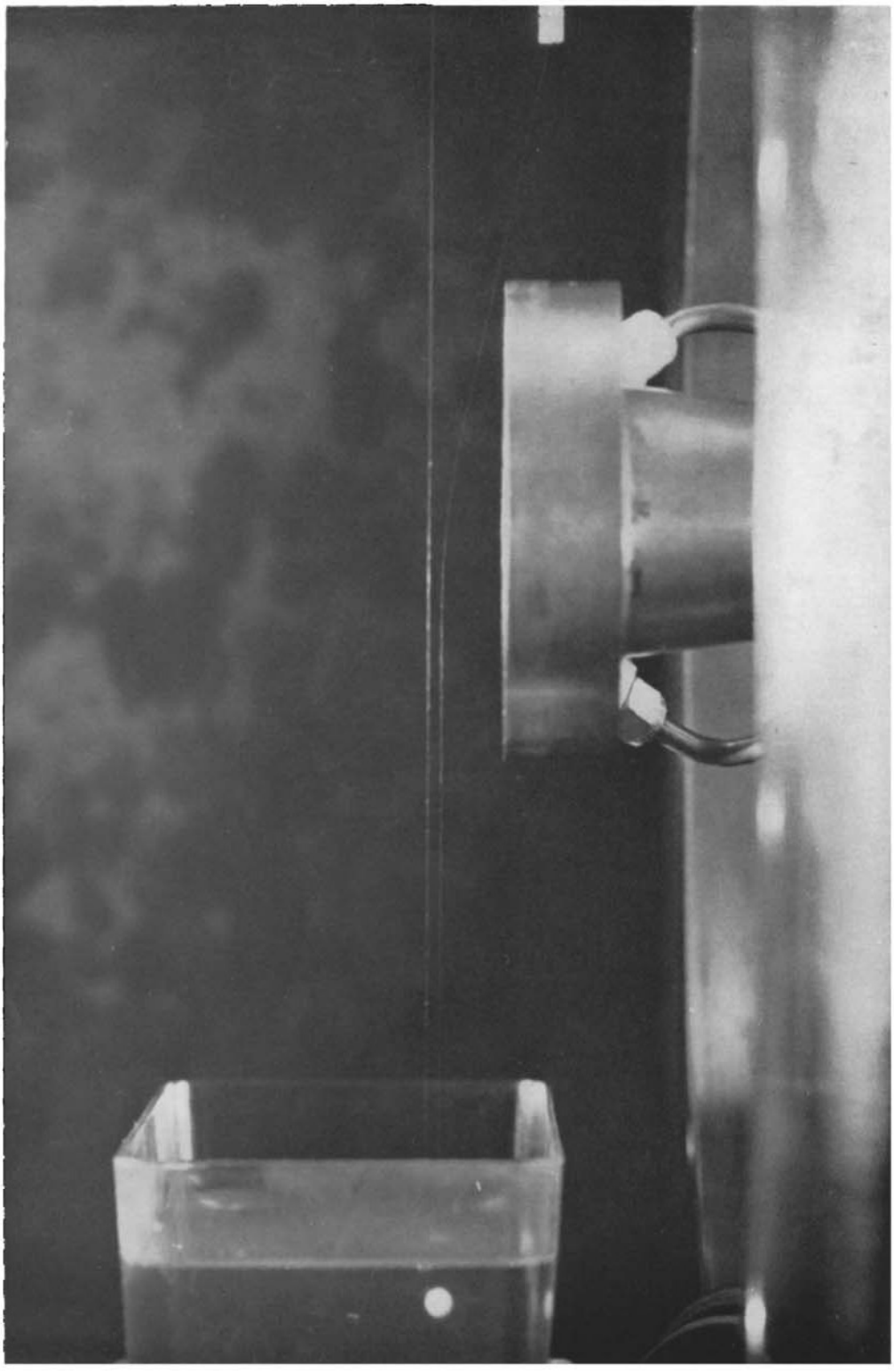

FIGURE 6. Support-wire drag determination.